



Two-dimensional vector bending sensor based on seven-core fiber Bragg gratings

MAOXIANG HOU,¹ KAIMING YANG,¹ JUN HE,^{1,2} XIZHEN XU,¹ SHUAI JU,¹ KUIKUI GUO,¹ AND YIPING WANG^{1,3}

¹Key Laboratory of Optoelectronic Devices and Systems of Ministry of Education and Guangdong Province, College of Optoelectronic Engineering, Shenzhen University, Shenzhen 518060, China

²hejun07@szu.edu.cn

³ypwang@szu.edu.cn

Abstract: We demonstrated a two-dimensional vector-bending sensor by use of fiber Bragg gratings (FBGs) inscribed in a homogeneous seven-core fiber. Seven FBGs were simultaneously inscribed in each of all seven cores using a modified Talbot interferometer and a lens scanning method. The vector bending response of six outer-core FBGs was investigated at all 360° directions with a step size of 15°. The bending sensitivities of the six outer-core FBGs display six perfect '8'-shaped patterns in a polar-coordinate system. That is, they exhibit strong bending-direction dependence with a maximum sensitivity of 59.47 pm/m⁻¹. The orientation and amplitude of the vector bending can be reconstructed using measured Bragg wavelength shifts of any two off-diagonal outer-core FBGs. So, the six outer-core FBGs have 12 combinations for bend reconstruction, which can be averaged across multiple reconstructions to develop an accurate two-dimensional vector bending sensor. The average relative error was lower than 4.5% for reconstructed amplitude and less than 2.8% for reconstructed orientation angle θ . Moreover, the seven-core FBGs offer several advantages such as a compact structure, fabrication flexibility, and the temperature compensating ability of central-core FBG.

© 2018 Optical Society of America under the terms of the [OSA Open Access Publishing Agreement](#)

OCIS codes: (060.3735) Fiber Bragg gratings; (060.2370) Fiber optics sensors.

1. Introduction

Vector bending sensors developed from optical fibers have been extensively investigated in recent years and have been implemented for a variety of applications, such as structural deformation, intelligent artificial limbs and mechanical engineering [1,2]. Vector bending sensors are usually divided into one- [3–10] and two-dimensional [11–14] sensors with different directional discrimination capabilities. One-dimensional bending sensors can only identify positive and negative directions by breaking cylindrical symmetry of the fiber. These include off-axis fiber Bragg gratings (FBGs) [3], eccentric FBGs [4,5], tilted FBGs [6], asymmetric long period fiber gratings (LPGs) [7–9], and lateral-offset Mach–Zehnder interferometers [1,10]. Two-dimensional bending sensors are usually constructed by combining two or more one-dimensional sensors in a particular alignment [11], such as two orthogonal LPGs [12] or orthogonal tilted FBGs [13]. However, orthogonal cascaded sensors require high precision alignment operations and can only identify limited axial directions. Additionally, two-dimensional bending sensors can also be produced by nesting multiple fibers grating together, which presents a significant packaging challenge [2,15,16].

Multicore fibers (MCFs) have developed rapidly in recent years due to exponential growth in data transmission requirements [17–19]. The use of vector bending sensors based on fiber gratings (FBGs or LPGs) in various MCFs has also been increasing, as the well-defined spatial distribution of different cores produces differential responses to fiber bend [20–27]. For instance, a one-dimensional bending sensor was produced by inscribing an FBG in one core of a twin-core few-mode fiber [22]. A two-dimensional bending sensor based on LPGs has also been proposed in three-core fibers [23]. There have been reports of vector bending

sensors based on seven-core FBGs [25], tilted FBGs [26] and LPGs [27]. However, conventional method for inscribing MCF-based gratings requires focusing a laser beam on one core for inscribing the first grating and then rotating the MCF by a certain angle for inscribing another grating on next core [27]. This method is always inefficient and destructive to the quality of gratings. Furthermore, it should be noted that not all cores in a MCF have been utilized for bend sensing in previous studies [25,26]. Hence, the approaches which can utilize all sensing channel and improve the vector bending measurement accuracy are still in demand.

In this study, we demonstrate the use of FBGs in seven-core fiber for two-dimensional vector bend sensing. These FBGs were inscribed in a homogeneous seven-core fiber using a modified Talbot interferometer [28] with a perpendicular lens scanning method. This makes it convenient for inscribed high quality FBGs in all cores without multiple-exposure. Each FBG exhibited a different response to vector bending due to the regular hexagon distribution of each core. The vector bending response of six-outer-core FBGs was investigated experimentally. Bending sensitivities at varying orientations were measured radially for display in a polar-coordinate system, achieving a maximum sensitivity of 59.47 pm/m^{-1} . The bending sensitivities of outer-core FBGs along a same diagonal line were almost equivalent with opposite directions, for a given bending orientation. Bend orientation and curvature amplitude could then be reconstructed based on the spectral shifts of any two off-diagonal outer-core FBGs. There are 12 combinations which can be used to reconstruct curvature for seven-core fiber (6 outer cores). These can be averaged across multiple reconstructions to acquire a more accurate value. The average relative error is lower than 4.5% for reconstructed amplitudes and less than 2.8% for the orientation angle θ . Seven-core FBGs offer several advantages such as a robust structure, fabrication flexibility, and the ability of two-dimensional vector bend sensing.

2. FBGs inscription in a seven-core fiber

The homogeneous seven-core fiber used in our experiments was fabricated by YOFC (Wuhan, China). Figure 1(a) shows a microscope image of the cross-section of a seven-core fiber which composed six outer cores and a central core. These six outer cores are distributed in a regular hexagon. Each fiber core consists of two layers: an inner core and an intermediate layer. The intermediate layer has a lower refractive index and is used as a depressed cladding trench to ensure mode isolation between adjacent fiber cores. The diameters of the inner core and fiber cladding are 8 and 150 μm , respectively. The distance between adjacent fiber cores is $\sim 42 \mu\text{m}$. Prior to FBGs inscription, the seven-core fiber was H_2 -loaded at 100 bar and 80 $^\circ\text{C}$ for 7 days to enhance its photosensitivity.

Figure 1(b) and 1(c) show the experimental configuration used for inscribing seven-core FBGs. The experimental setup is composed of a modified Talbot interferometer with a scanning lens. A uniform phase mask (Ibsen Photonics) with a period of 1069 nm, was designed for zero order suppression at 266 nm wavelength and used as a beam splitter. The ± 1 th beams are then redirected to interfere in the fiber core by two rotation mirrors, and used for FBGs inscription. A short-focal-length cylindrical lens was positioned in front of the interference area and was used to increase the power density in this area. The period of the interference pattern (the grating period) can be determined by [28]:

$$\Lambda = \frac{\lambda_{\text{laser}}}{2 \sin(\alpha + 2\varphi)}, \quad (1)$$

where λ_{laser} is the laser wavelength, φ is the rotation angle of the mirrors, and α is the ray deviation angle for the +1 and 0-order diffraction peaks located after the phase mask. In this study, α is 14.408° . This approach is stable and allows for the inscription of FBGs with variable Bragg wavelengths applied in WDM system.

A CW laser source (Coherent, Verdi G-5W 532 nm) with a second harmonic generator (SHG, Coherent, model MBD) is used to produce an ultraviolet (UV) laser for FBG inscription. The laser beam has a $1/e^2$ Gaussian diameter of 4 mm, a power of 100 mW, and a wavelength of 266 nm. As shown in Fig. 1(b), the laser beam was focused onto the seven-core fiber using a cylindrical lens with a focal length of 25 mm. The focal width and Rayleigh length of the laser beam were calculated (using Gaussian beam optics) to be 2.11 and 13.23 μm , respectively. A perpendicular scanning was implemented for the cylindrical lens (i.e. along z axis shown in Fig. 1(b)), with a speed of 0.002 mm/s and a scanning length of 0.2 mm, to ensure that FBG can be inscribed in all seven cores without multiple-exposure.

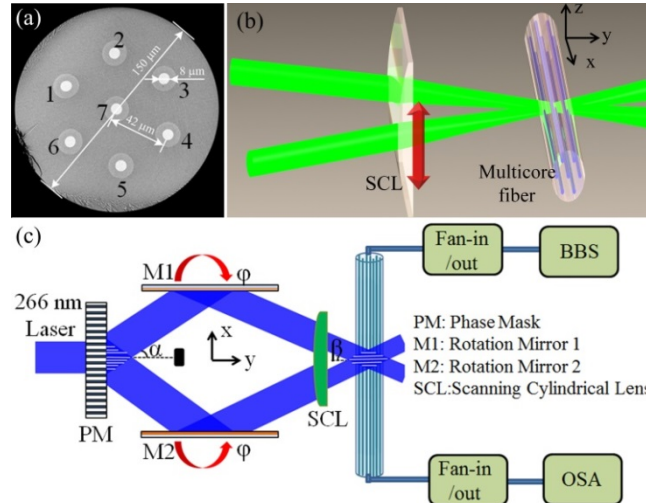


Fig. 1. A schematic diagram of the seven-core FBG inscription process using a scanning UV laser. (a) Microscopic image of the cross-section of the seven-core fiber. (b) A schematic of the seven-core FBGs inscription using a modified Talbot interferometer with a perpendicular scanning cylindrical lens. (c) The experimental setup.

After FBGs inscription, the transmission and reflection spectra of the seven-core FBGs were measured using a broadband light source (BBS) together with an optical spectrum analyzer (OSA, Yokagawa AQ6370C) and two fan-in/out devices (YOFC). As shown in Fig. 2(a) and 2(b), seven FBGs were successfully inscribed into the seven cores of the MCF with similar Bragg wavelengths of $\lambda_B = 1550.04, 1550.48, 1550.65, 1550.15, 1549.41, 1549.77,$ and 1550.2 nm, and resonance loss at λ_B of $-7.18, -2.86, -9.58, -8.61, -4.87, -4.77,$ and -5.65 dB, respectively. It is worth noting that, the Bragg wavelengths of these FBGs are slightly different from each other. This should result from the uneven UV exposure formed by the focusing effect of the circular fiber cladding layer [29,30].

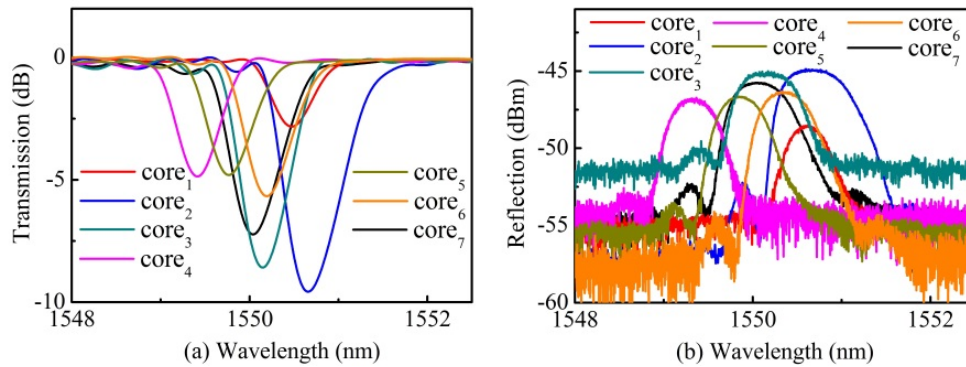


Fig. 2. Transmission spectra (a) and reflection spectra (b) of the FBGs inscribed in a seven-core fiber.

3. Two-dimensional vector bending experiments

We investigated two-dimensional bending response of the seven-core FBGs via the experimental setup shown in Fig. 3(a). Firstly, the seven-core fiber, which contained the seven-core FBGs, was spliced with a fan-in/out device and then connected with a multi-channel demodulator (B&A FT210-08) to measure its reflection spectra. The seven-core FBGs were then mounted on a pair of 3D translation stages by two rotary fiber holders (Newport model 466A-718). The bending curvature could be changed by moving the translation stages. In addition, the bending orientation could be changed by simultaneous rotating the two rotary fiber holders. As shown in Fig. 3(b) and 3(c), the bend orientation angle θ was defined as the included angle between the bending plane and the axis connecting core₁ and core₄ in the seven-core fiber. In case θ equals 0° or 360° , the bending orientation coincided with the core₁ and core₄ axis, and core₁ was located on the outer side of the bent seven-core fiber. It is important to point out that the initial angle ($\theta = 0^\circ$) alignment of the MCF was performed simply by detecting its near-mode field patterns through a CCD camera. Finally, the FBG reflection spectra were recorded as bend measurements were conducted.

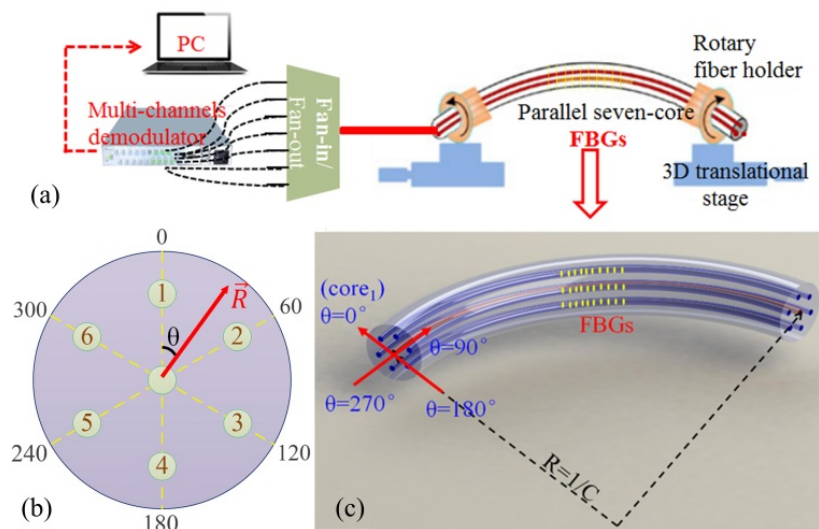


Fig. 3. Schematic images of directional bend measurements for the seven-core FBGs. (a) The experimental setup. (b) and (c): The bend orientation (θ) with respect to seven-core FBGs coinciding with the core₁ and core₄ axes. Core₁ was located on the outer side of the bent MCF.

First, the curvature of the seven-core FBGs was set by adjusting the distance between two translation stages. Subsequently, the bending orientation of the seven-core FBGs was set by simultaneously adjusting the rotary fiber holders with a step of 15° . It should also be noted that fiber twisting should be avoided during bending measurements. The wavelength shifts in the reflection spectra were recorded for each FBG at various orientation angles.

When located at the outer side of the bending seven-core fiber, the outer-core FBG will be stretched which results a shift to longer wavelengths (i.e. ‘red’ shift). On the contrary, when located at the inner side, the outer-core FBG will be compressed which results in a shift to shorter wavelengths (i.e. ‘blue’ shift). However, tiny bend-induced strain applied to the central-core FBG (i.e. core₇) when the seven-core fiber is bend, which makes its insensitive to bending [19]. Thus, the central-core FBG can be used to compensate temperature-induced wavelength shift, which overcomes the cross-sensitivity problem between bend and temperature in the bend sensing applications [25].

Results for two FBGs along the same diagonal line (i.e. FBG₁ and FBG₄) are shown in Figs. 4(a) and 4(b) for increasing curvature. A linear fit was applied to all shifts in the Bragg wavelength at given angles θ , with the slope representing bend sensitivity. Figures 4(c) and 4(d) show Bragg wavelength shifts for FBG₁ and FBG₄ with increasing orientation angles. All shifts for a given curvature show good agreement with sinusoidal behavior [22]. As shown in Fig. 4(a), FBG₁ had the highest positive sensitivity (59.47 pm/m^{-1}) at 0° and the highest negative sensitivity (-55.49 pm/m^{-1}) at 180° . However, FBG₁ had the lowest sensitivity approaching to zero at 90° and 270° . In contrast, as shown in Fig. 4(b), FBG₄ had the highest negative sensitivity (-56.34 pm/m^{-1}) at 0° and the highest positive sensitivity (55.49 pm/m^{-1}) at 180° . The bend sensitivity of FBG₄ reached a minimum and approached zero for θ equal to 90° and 270° . Above all, the results reveal that the bend sensitivities of two outer-core FBGs along a same diagonal line have a similar amplitude and opposite directionality.

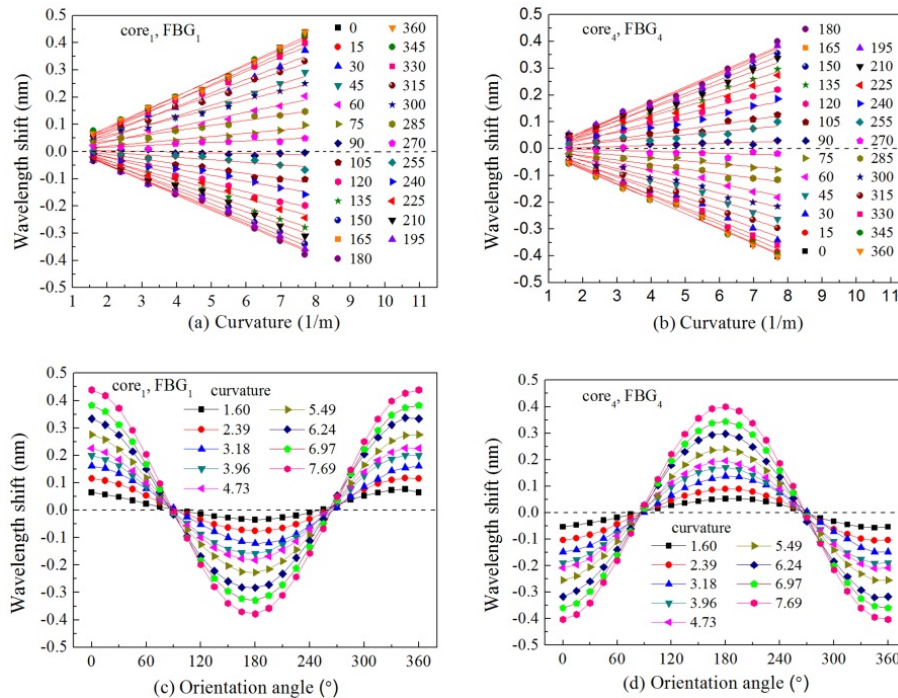


Fig. 4. Measured Bragg wavelength shifts plotted against curvature for different orientations: (a) FBG₁ and (b) FBG₄. Also shown are measured Bragg wavelength shifts for (c) FBG₁ and (d) FBG₄, plotted as a function of the bend direction angle θ .

Bend sensitivities were obtained from the linear fits for FBG₁ and FBG₄ at different orientations and are displayed in polar coordinates in Fig. 5. Strong angular dependence of the bending response was achieved and two perfect '8'-shaped patterns are clearly visible. The sensitivity of FBG₁ was positive during stretching when the bending orientation angle was in the range of 270°–0°–90°. In contrast, the sensitivity was negative during compression while in the range of 90°–180°–270°. The bend sensitivity of FBG₁ achieved its maximum value for angles equal to 0° and 180° (i.e., the bend direction along the diagonal line of core₁ and core₄), while reached a minimum and approached zero in the case of θ equal to 90° and 270° (i.e., the bend direction perpendicular to the diagonal of core₁ and core₄). Moreover, at a same bend orientation, the sensitivity amplitude of FBG₄ is very close to that of FBG₁ and the direction is completely opposite. There are slight differences in sensitivity amplitudes of these two FBGs, which may be due to fine measurement errors. The two substantially coincident '8'-shaped patterns suggest the seven-core fiber maintains good circular symmetry during bending. The angular-dependent bending sensitivity of these seven-core FBGs supports their potential for use in vector bend sensing.

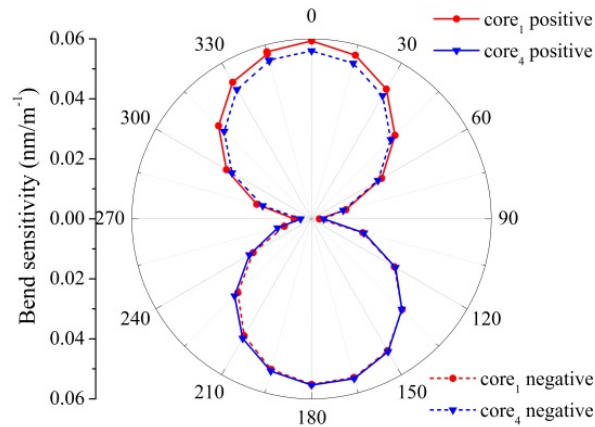


Fig. 5. Bend sensitivities for two FBGs in the seven-core FBGs (i.e. FBG₁ and FBG₄) plotted for various bend directions (from 0° to 360°).

Furthermore, the bending responses of the other four outer-core FBGs (i.e. FBG₂, FBG₃, FBG₅ and FBG₆) were analyzed. As shown in Fig. 6, there are six '8'-shaped patterns corresponding to the six outer-core FBGs. Each '8'-shaped pattern includes two maxima and two minima. Maximum sensitivities were achieved when the bending axis was coincides with the FBG plates, while minimum sensitivities occurred with the bending axis in the orthogonal direction. Similarly, the two FBGs along a same diagonal line have almost the same bending sensitivities and opposite directions. The maximum positive sensitivity for each outer-core FBG was 59.47, 57.35, 57.08, 55.49, 56.28, and 57.13 pm/m⁻¹ (K₁, K₂, K₃, K₄, K₅, and K₆), with corresponding azimuths of 0°, 60°, 120°, 180°, 240°, and 300°, respectively. This sensitivity of each FBG varied slightly due to the differences in fabrication processes and embedded sensor depths. Two-dimensional curvature reconstruction could then be achieved during vector bend solving using the maximum sensitivity of each FBG (K₁, K₂, K₃, K₄, K₅, and K₆) and the regular hexagon geometric relationship between individual cores.

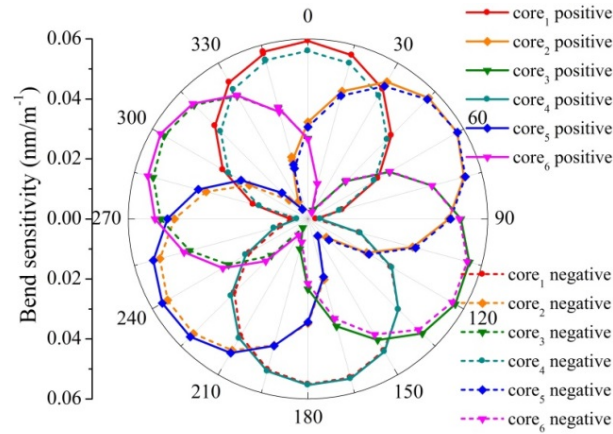


Fig. 6. Bend sensitivities for the six outer-core FBGs in the seven-core FBGs (i.e., core₁, core₂, core₃, core₄, core₅ and core₆) plotted for various bend directions (from 0° to 360°).

4. Curvature reconstruction

In order to reconstruct the orientation and amplitude of the bending vector \vec{R} , we assumed the cross section of the seven-core fiber maintained a circular shape. The Bragg wavelength shift $\Delta\lambda$ of each FBG is the first-hand data that can be measured during bending measurements. From the relationship $R = \Delta\lambda/S$ (S is the bend sensitivity come from Fig. 6)

[2], the vector components \vec{r}_n of the bending vector \vec{R} projected on the six outer-core FBGs can be expressed as:

$$\vec{r}_n = \frac{\Delta\lambda_n}{K_n} \vec{e}_n, \quad (2)$$

where $n = 1, 2, \dots, 6$. Subsequently, the bending vector \vec{R} could be reconstructed from these vector components \vec{r}_n using geometric positional relationship between these FBGs in the

seven-core fiber. As shown in Figs. 7, the bending vector \vec{R} was projected on three diagonal lines, in four different quadrants. Note that, in theory, the bending components of two outer-core FBGs along a same diagonal line are equal in amplitude but in opposite directions ($\vec{r}_1 = -\vec{r}_4, \vec{r}_2 = -\vec{r}_5, \vec{r}_3 = -\vec{r}_6$). Actually, their obtained amplitudes vary slightly due to some fine measurement errors. It is also worth noting that the orientation and amplitude of the

bending vector \vec{R} could be reconstructed based on the spectra shifts of any two off-diagonal outer-core FBGs. This theoretical analysis can be extended to different core combinations using the corresponding regular hexagon geometric relationships between the positions of each core. So, there are 12 combinations which can be used to reconstruct curvature for seven-core fibers (6 outer cores). They can be averaged across multiple reconstructions to achieve a more accurate value.

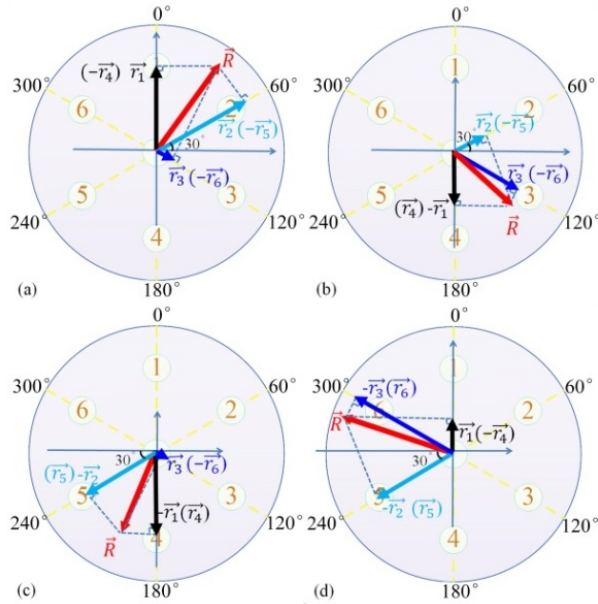


Fig. 7. A schematics diagram of the bending vector \vec{R} in different quadrants and decomposed into three components along three diagonal lines: (a) quadrant I, (b) quadrant II, (c) quadrant III, and (d) quadrant V.

For example, in quadrant I, as shown in Fig. 7(a), \vec{r}_1 , \vec{r}_2 , and \vec{r}_3 were the components of the bending vector \vec{R} projected onto three diagonal lines, respectively. According to Eq. (2), \vec{r}_1 , \vec{r}_2 , and \vec{r}_3 could be calculated from the specific Bragg wavelength shifts $\Delta\lambda_n$. And then, using the regular hexagon geometric relationship between these FBGs, the orientation and amplitude of bending vector \vec{R} can be calculated using any two of the three components. So that, there are 3 combinations (i.e. (\vec{r}_1, \vec{r}_2) , (\vec{r}_1, \vec{r}_3) and (\vec{r}_2, \vec{r}_3)) for reconstruct \vec{R} which can be expressed as follows:

$$|\vec{R}| = \begin{cases} \sqrt{|\vec{r}_1|^2 + y_1^2} \\ \sqrt{|\vec{r}_1|^2 + y_2^2} \\ \sqrt{|\vec{r}_2|^2 + y_3^2} \end{cases} \quad (3)$$

Here y_1, y_2 , and y_3 can be expressed as:

$$y_1 = \frac{2\sqrt{3}\vec{r}_2}{3} - \frac{\sqrt{3}\vec{r}_1}{3}, \quad (4)$$

$$y_2 = \frac{2\sqrt{3}\vec{r}_3}{3} + \frac{\sqrt{3}\vec{r}_1}{3}, \quad (5)$$

$$y_3 = \frac{\sqrt{3}\bar{r}_2}{3} - \frac{2\sqrt{3}\bar{r}_3}{3}, \tag{6}$$

The corresponding orientation angle θ can be determined by:

$$\theta = \begin{cases} \arctan\left(\frac{y_1}{r_1}\right), \\ \arctan\left(\frac{y_2}{r_1}\right), \\ \arctan\left(\frac{\bar{r}_2}{y_3}\right) - \frac{\pi}{6}, & (0 \sim \frac{\pi}{3}) \\ \frac{5\pi}{6} - \arctan\left(\frac{\bar{r}_2}{y_3}\right), & (\frac{\pi}{3} \sim \frac{\pi}{2}) \end{cases} \tag{7}$$

Note that in Eq. (3) to Eq. (7), \bar{r}_1 , \bar{r}_2 , and \bar{r}_3 can be replaced by $-\bar{r}_4$, $-\bar{r}_5$, and $-\bar{r}_6$, respectively. This constitutes 12 combinations which can be used to reconstruct the bending vector \vec{R} , namely (\bar{r}_1, \bar{r}_2) , (\bar{r}_1, \bar{r}_3) , (\bar{r}_1, \bar{r}_5) , (\bar{r}_1, \bar{r}_6) , (\bar{r}_4, \bar{r}_2) , (\bar{r}_4, \bar{r}_3) , (\bar{r}_4, \bar{r}_5) , (\bar{r}_4, \bar{r}_6) , (\bar{r}_2, \bar{r}_3) , (\bar{r}_2, \bar{r}_6) , (\bar{r}_3, \bar{r}_5) and (\bar{r}_5, \bar{r}_6) .

We tested the reconstruction performance of seven-core FBGs using a set of sampled data. For a set of given conditions ($|\vec{R}| = 6.095$, $\theta = 30^\circ$), the measured Bragg wavelength shifts ($\Delta\lambda_n$) of the six outer-core FBGs were -0.324 , -0.325 , -0.005 , 0.302 , 0.311 , and 0.002 nm, respectively. The curvature components \bar{r}_n for these FBGs are calculated by using Eq. (2) as -5.446 , -5.661 , -0.088 , 5.430 , 5.525 and 0.034 m⁻¹, respectively. The curvature $|\vec{R}|$ can be reconstructed using Eq. (3) to Eq. (7), as shown in Table 1.

Table 1. The results of curvature (6.095 m⁻¹, 30°) reconstructed for 12 different combinations.

Reconstructed combination	$ \vec{R} = 6.095$		Reconstructed combination	$ \vec{R} = 6.095$	
	(m ⁻¹)	$\theta = 30^\circ$		(m ⁻¹)	$\theta = 30^\circ$
(\bar{r}_1, \bar{r}_2)	6.416	31.92	(\bar{r}_4, \bar{r}_5)	6.326	30.89
(\bar{r}_1, \bar{r}_3)	6.340	30.79	(\bar{r}_4, \bar{r}_6)	6.290	30.31
(\bar{r}_1, \bar{r}_5)	6.334	30.72	(\bar{r}_2, \bar{r}_3)	6.486	30.79
(\bar{r}_1, \bar{r}_6)	6.308	30.31	(\bar{r}_2, \bar{r}_6)	6.517	30.30
(\bar{r}_4, \bar{r}_2)	6.408	31.06	(\bar{r}_3, \bar{r}_5)	6.330	30.80
(\bar{r}_4, \bar{r}_3)	6.322	30.80	(\bar{r}_5, \bar{r}_6)	6.399	30.39
Average	6.373	30.84			

The averaged reconstruction results of 12 different combinations (6.373 m^{-1} , 30.84°) was very close to the actual curvature and bend direction (6.095 m^{-1} , 30°). The average relative error was lower than 4.5% for reconstructed amplitudes and less than 2.8% for the orientation angle θ . These relative errors were lower than prior studies based on seven-core fiber [25,31]. Moreover, it should be noted that the averaged values obtained by multiple reconstructions can counteract measurement errors and provide more accurate results. Subsequently, we used this method to perform three sets of curvature reconstruction in different quadrants.

Table 2. The curvature reconstruction results for bending vectors in 4 different quadrants.

Actual Value	(0.794 m^{-1} , 30.00°)	(2.363 m^{-1} , 30.00°)	(6.095 m^{-1} , 30.00°)
Reconstructed Value	(0.875 m^{-1} , 30.06°)	(2.332 m^{-1} , 33.75°)	(6.373 m^{-1} , 30.84°)
Actual Value	(0.794 m^{-1} , 120.00°)	(2.363 m^{-1} , 120.00°)	(6.095 m^{-1} , 120.00°)
Reconstructed Value	(0.666 m^{-1} , 117.95°)	(2.11 m^{-1} , 122.55°)	(6.058 m^{-1} , 121.02°)
Actual Value	(0.794 m^{-1} , 210.00°)	(2.363 m^{-1} , 210.00°)	(6.095 m^{-1} , 210.00°)
Reconstructed Value	(0.730 m^{-1} , 212.07°)	(2.108 m^{-1} , 214.09°)	(6.119 m^{-1} , 212.78°)
Actual Value	(0.794 m^{-1} , 300.00°)	(2.363 m^{-1} , 300.00°)	(6.095 m^{-1} , 300.00°)
Reconstructed Value	(0.805 m^{-1} , 303.19°)	(2.223 m^{-1} , 302.49°)	(6.133 m^{-1} , 301.07°)

It could be seen clearly from Table 2 that the seven-core FBGs can be used as a two-dimensional vector bending sensor to reconstruct the orientation and curvature of bending vectors, with accurate accordance values. For a given orientation angle θ , larger curvatures will result in smaller relative reconstruction errors. However, reconstructions of the orientation angle did not show a specific tendency.

5. Conclusion

We have proposed and demonstrated a two-dimensional bend sensor utilizing FBGs which were inscribed in a homogeneous seven-core fiber using a modified Talbot interferometer with a perpendicular lens scanning method. The bending responses of six outer-core FBGs were investigated in all 360° directions with a step size of 15° . Strong angular dependences were observed in the bend sensitivities of outer-core FBGs, with a maximum sensitivity of 59.47 pm/m^{-1} . The orientation and amplitude of curvature could be reconstructed using the acquired Bragg wavelength shifts and the regular hexagon geometric relationship between each core. For seven-core fibers, there are 12 combinations that can be used to reconstruct curvature. For a specific set of conditions curvature ($|\vec{R}| = 6.095$, $\theta = 30^\circ$), the reconstructed average value of 12 different combinations was (6.373 m^{-1} , 30.84°), with a relative error of 4.5% for amplitudes and 2.8% for the orientation angle θ . These seven-core fiber-based FBGs are capable of two-dimensional vector bend sensing and have significant potential for intelligent artificial limb applications.

Funding

National Natural Science Foundation of China (NSFC) (61875128, 61505120, 61425007, 61635007); Natural Science Foundation of Guangdong Province (2017A010102015, 2015B010105007, 2014A030308007); Science and Technology Innovation Commission of Shenzhen (JCYJ20170302154614941, JCYJ20170302143105991, JCYJ20170412105604705, JCYJ20160427104925452, JCYJ20160307143716576); China Postdoctoral Science Foundation (2017M612720, 2016M600669), Research Funding from Shenzhen University (2017019, 2016030), and Development and Reform Commission of Shenzhen Municipality Foundation.

References

1. Z. Ou, Y. Yu, P. Yan, J. Wang, Q. Huang, X. Chen, C. Du, and H. Wei, "Ambient refractive index-independent bending vector sensor based on seven-core photonic crystal fiber using lateral offset splicing," *Opt. Express* **21**(20), 23812–23821 (2013).
2. L. Xu, J. Ge, J. H. Patel, and M. P. Fok, "Dual-layer orthogonal fiber Bragg grating mesh based soft sensor for 3-dimensional shape sensing," *Opt. Express* **25**(20), 24727–24734 (2017).
3. D. Feng, X. Qiao, and J. Albert, "Off-axis ultraviolet-written fiber Bragg gratings for directional bending measurements," *Opt. Lett.* **41**(6), 1201–1204 (2016).
4. X. Chen, C. Zhang, D. J. Webb, K. Kalli, and G. D. Peng, "Highly sensitive bend sensor based on Bragg grating in eccentric core polymer fiber," *IEEE Photonics Technol. Lett.* **22**(11), 850–852 (2010).
5. W. Bao, Q. Rong, F. Chen, and X. Qiao, "All-fiber 3D vector displacement (bending) sensor based on an eccentric FBG," *Opt. Express* **26**(7), 8619–8627 (2018).
6. L. Y. Shao, L. Y. Xiong, C. K. Chen, A. Laronche, and J. Albert, "Directional bend sensor based on re-grown tilted fiber Bragg grating," *J. Lightwave Technol.* **28**(18), 2681–2687 (2010).
7. B. Jiang, Z. Bai, C. Wang, Y. Zhao, J. Zhao, L. Zhang, and K. Zhou, "In-line Mach-Zehnder interferometer with D-shaped fiber grating for temperature-discriminated directional curvature measurement," *J. Lightwave Technol.* **36**(3), 742–747 (2018).
8. L. Jin, W. Jin, and J. Ju, "Directional bend sensing with a CO₂-laser-inscribed long period grating in a photonic crystal fiber," *J. Lightwave Technol.* **27**(21), 4884–4891 (2009).
9. X. Zhong, C. Guan, G. Mao, J. Fu, Y. Liu, J. Shi, and L. Yuan, "Bending characteristics of a long-period fiber grating in a hollow eccentric optical fiber," *Appl. Opt.* **54**(26), 7879–7883 (2015).
10. S. Zhang, W. Zhang, S. Gao, P. Geng, and X. Xue, "Fiber-optic bending vector sensor based on Mach-Zehnder interferometer exploiting lateral-offset and up-taper," *Opt. Lett.* **37**(21), 4480–4482 (2012).
11. Y. P. Wang and Y. J. Rao, "A novel long period fiber grating sensor measuring curvature and determining bend direction simultaneously," *IEEE Sens. J.* **5**(5), 839–843 (2005).
12. P. Geng, W. Zhang, S. Gao, H. Zhang, J. Li, S. Zhang, Z. Bai, and L. Wang, "Two-dimensional bending vector sensing based on spatial cascaded orthogonal long period fiber," *Opt. Express* **20**(27), 28557–28562 (2012).
13. D. Feng, W. Zhou, X. Qiao, and J. Albert, "Compact optical fiber 3d shape sensor based on a pair of orthogonal tilted fiber Bragg gratings," *Sci. Rep.* **5**(1), 17415 (2015).
14. J. Kong, A. Zhou, C. Cheng, J. Yang, and L. Yuan, "Two-axis bending sensor based on cascaded eccentric core fiber Bragg gratings," *IEEE Photonics Technol. Lett.* **28**(11), 1237–1240 (2016).
15. H. Wang, R. Zhang, W. Chen, and X. Liang, X., and R. Pfeifer, "Shape detection algorithm for soft manipulator based on fiber bragg gratings," *IEEE/ASME T. Mech.* **21**(6), 2977–2982 (2016).
16. F. Parent, S. Loranger, K. K. Mandal, V. L. Iezzi, J. Lapointe, J. S. Boisvert, M. D. Baiad, S. Kadoury, and R. Kashyap, "Enhancement of accuracy in shape sensing of surgical needles using optical frequency domain reflectometry in optical fibers," *Biomed. Opt. Express* **8**(4), 2210–2221 (2017).
17. D. J. Richardson, J. M. Fini, and L. E. Nelson, "Space-division multiplexing in optical fibres," *Nat. Photonics* **7**(5), 354 (2013).
18. B. Zhu, T. F. Taunay, M. F. Yan, J. M. Fini, M. Fishteyn, E. M. Monberg, and F. V. Dimarcello, "Seven-core multicore fiber transmissions for passive optical network," *Opt. Express* **18**(11), 11117–11122 (2010).
19. A. Donko, M. Beresna, Y. Jung, J. Hayes, D. J. Richardson, and G. Brambilla, "Point-by-point femtosecond laser micro-processing of independent core-specific fiber Bragg gratings in a multi-core fiber," *Opt. Express* **26**(2), 2039–2044 (2018).
20. H. Zhang, Z. Wu, P. P. Shum, R. Wang, X. Q. Dinh, S. Fu, W. Tong, and M. Tang, "Fiber Bragg gratings in heterogeneous multicore fiber for directional bending sensing," *J. Opt.* **18**(8), 085705 (2016).
21. G. Mao, T. Yuan, C. Guan, J. Yang, L. Chen, Z. Zhu, J. Shi, and L. Yuan, "Fiber Bragg grating sensors in hollow single- and two-core eccentric fibers," *Opt. Express* **25**(1), 144–150 (2017).
22. K. Yang, J. He, C. Liao, Y. Wang, S. Liu, K. Guo, J. Zhou, Z. Li, Z. Tan, and Y. Wang, "Femtosecond laser inscription of fiber Bragg grating in twin-core few-mode fiber for directional bend sensing," *J. Lightwave Technol.* **35**(21), 4670–4676 (2017).
23. S. Wang, W. Zhang, L. Chen, Y. Zhang, P. Geng, Y. Zhang, T. Yan, L. Yu, W. Hu, and Y. Li, "Two-dimensional microbend sensor based on long-period fiber gratings in an isosceles triangle arrangement three-core fiber," *Opt. Lett.* **42**(23), 4938–4941 (2017).
24. G. M. H. Flockhart, W. N. MacPherson, J. S. Barton, J. D. C. Jones, L. Zhang, and I. Bennion, "Two-axis bend measurement with Bragg gratings in multicore optical fiber," *Opt. Lett.* **28**(6), 387–389 (2003).
25. D. Zheng, J. Madrigal, H. Chen, D. Barrera, and S. Sales, "Multicore fiber-Bragg-grating-based directional curvature sensor interrogated by a broadband source with a sinusoidal spectrum," *Opt. Lett.* **42**(18), 3710–3713 (2017).
26. D. Barrera, J. Madrigal, and S. Sales, "Tilted fiber Bragg gratings in multicore optical fibers for optical sensing," *Opt. Lett.* **42**(7), 1460–1463 (2017).
27. D. Barrera, J. Madrigal, and S. Sales, "Long period gratings in multicore optical fibers for directional curvature sensor implementation," *J. Lightwave Technol.* **36**(4), 1063–1068 (2018).

28. Y. Wang, J. Grant, A. Sharma, and G. Myers, "Modified Talbot interferometer for fabrication of fiber-optic grating filter over a wide range of Bragg wavelength and bandwidth using a single phase mask," *J. Lightwave Technol.* **35**(21), 4670–4676 (2001).
29. E. Lindley, S. S. Min, S. Leon-Saval, N. Cvetojevic, J. Lawrence, S. Ellis, and J. Bland-Hawthorn, "Demonstration of uniform multicore fiber Bragg gratings," *Opt. Express* **22**(25), 31575–31581 (2014).
30. Y. Lai, K. Zhou, K. Sugden, and I. Bennion, "Point-by-point inscription of first-order fiber Bragg grating for C-band applications," *Opt. Express* **15**(26), 18318–18325 (2007).
31. Z. Zhao, M. A. Soto, M. Tang, and L. Thévenaz, "Distributed shape sensing using Brillouin scattering in multicore fibers," *Opt. Express* **24**(22), 25211–25223 (2016).